International Journal of Biological Macromolecules 170 (2021) 572–582

Contents lists available at ScienceDirect

International Journal of Biological Macromolecules

journal homepage: http://www.elsevier.com/locate/ijbiomac

Dual ionic liquid-based crosslinked chitosan for fine-tuning of antifouling, water throughput, and denitrification performance of polysulfone membrane

Reda F.M. Elshaarawy [a,b,*], Reda M. Abd El-Aal [a], Fatma H.A. Mustafa [c], Ahmed E. Borai [a], Stephan Schmidt [d], Christoph Janiak [b]

[a] Faculty of Science, Suez University, Suez, Egypt
[b] Institut für Anorganische Chemie und Strukturchemie, Heinrich-Heine Universität Düsseldorf, 40204 Düsseldorf, Germany
[c] Marine Chemistry Laboratory, Marine Environment Division, National Institute of Oceanography and Fisheries (NIOF), Suez, Egypt
[d] Department of Colloidal Adhesion, Organic and Macromolecular Chemistry Institute, Heinrich-Heine Universität Düsseldorf, 40225 Düsseldorf, Germany

ARTICLE INFO

Article history:
Received 8 October 2020
Received in revised form 13 December 2020
Accepted 23 December 2020
Available online 29 December 2020

Keywords:
Mixed-matrix membranes
Poly(ionic) crosslinked chitosan Schiff bases
Denitrification process performance

ABSTRACT

This study aimed to design a facile and efficient protocol for upgrading the performance indices of polysulfone (PS) membrane (porosity, hydrophilicity, pure water flux (PWF), surface charge, and fouling-resistance) by blending with newly synthesized poly(ionic) crosslinked chitosan Schiff bases (PICCSBs). The PS-PICCSBs mixed-matrix membranes (MMMs) have successfully fabricated and characterized based on spectral and microscopic analyses, porosity, zeta potential, water contact angle, and water uptake (wettability) measurements. The PWF, fouling-resistance against bovine serum albumin (BSA), as well as ion exchange capacity (IEC) against nitrate anion were studied. The wettability, hydrophilicity and overall porosity of new MMMs have greatly increased, in comparison to a pristine PS membrane (M_0). In addition, blending of PS with PICCSBs resulted in switching its surface from negatively- to positively-charged. The PWF of MMMs has increased to reach a maximum value of 238.6 L/m^2 h for MMM_1 (9.3-fold higher than M_0). Meanwhile, BSA rejection has declined from 96.62% for M_0 to 41.9% for MMM_1. The fouling parameters results of MMMs indicated their low fouling propensity. The IEC of nitrate anions revealed that the nitrate uptake by MMM_1 is higher than that for M_0 and MMM_2 by 34% and 14%, respectively.

1. Introduction

During the last few decades, freshwater resources were remarkably diminished in several areas of the world [1]. This problem can be expected to aggravate as a result of multiple factors such as population growth, water contamination, climate change, and abuse of water resources, leading to a freshwater scarcity problem [1–3]. The World Water Council (WWC) predicts that, by the end of 2030, 3.9 billion people will strongly suffer from water scarcity, around the world [4]. Therefore, water scarcity is a dormant crisis about to burst worldwide. Consequently, there is an urgent need for developing simple, efficient, and feasible technologies for wastewater remediation.

Membrane technologies are preferred over many other technologies for water remediation owing to their unmatched features including economic, selective, mild operating conditions, efficiency, no need for chemical or thermal treatments, reliable purification, and eco-friendship [5]. In the last few decades, membrane technology has developed with the integration of filtration and adsorption processes [6,7]. Membrane-coated adsorbents were effectively applied in water desalination and removal of hazardous pollutants including heavy metal ions, anions, toxic organic compounds, and dyes from wastewater [8–10].

The excellent thermal and chemical stability, superior mechanical properties, and good film-forming characteristic of polysulfone (PS) [11–13], have attracted the attention of many membrane-interested researchers. The main drawbacks of PS membranes are the inherent hydrophobicity and non-wetting properties which facilitate the hydrophobic interaction and deposition of microorganisms and/or organic pollutants from the feed solution onto their surfaces, causing serious membrane biofouling [13–15], and consequently, poor permeation, diminishing water flux, and defects in the selectivity and durability of membrane. Both physical and chemical modifications can be applied to overcome these disadvantages. Using polymeric additives, dendrimers, inorganic fillers, inorganic nanoparticles, and carbon

* Corresponding author at: Faculty of Science, Suez University, Suez, Egypt.
E-mail addresses: reda.elshaarawy@suezuniv.edu.eg, reel-001@hhu.de (R.F.M. Elshaarawy).

https://doi.org/10.1016/j.ijbiomac.2020.12.186
0141-8130/

nanomaterials during PS membrane fabrication, has been attracted a significant attention to enhance its hydrophilicity, antifouling properties, and performance [13,16,17].

Amongst membrane polymeric additives for water treatment, chitosan has been getting considerable attention [13,18,19], due to its eco-friendship, higher hydrophilicity, unique perm-selectivity for water [20], perfect thin film-forming ability, biodegradability, non-toxicity, acceptable anti-biofilm and antifouling properties [21], and dual ionic nature as it can be positively or negatively charged in an acidic or alkaline medium, respectively [22]. This charge fluctuation plays a key role in the performance of the membrane [23]. However, the main disadvantages of native chitosan membrane such as poor acid stability, substandard mechanical characteristics [24], and low porosity and surface area [8], restrict their widespread applications in the water treatments. Again, physical and chemical refinements can be utilized to address these drawbacks. Chemical amendments can significantly enhance the chemomechanical stability of chitosan; however, these refinements usually are at the expense of its adsorption capacity, due to blocking of active adsorptive sites (amino groups). To overcome this problem, surface modification of chitosan with multifunctional modulators such as Schiff base segments can be used. The grafting of chitosan with Schiff bases enhanced its mechanical [25], antimicrobial, wettability and antifouling properties [25,26], and adsorptive capacity [27,28], as well. Moreover, supporting the surfaces of chitosan Schiff bases (CSBs) by ionic liquid terminals has significantly promoted their antimicrobial, anti-biofilm, and anti-biofouling properties [26,29,30].

Consequently, incorporation of polymeric additives (poly(ionic liquid) chitosan Schiff bases (PILCSBs)) into the matrix of polysulfone (PS) membrane could provide an opportunity to design mixed-matrix membranes (MMMs) with improved hydrophilicity and better performance in terms of permeability, porosity, and rejection ability. Elshaarawy et al. have fabricated PS/PILCSBs/titania nanoparticle (TNP) MMMs with a three-fold higher wettability than that of a pristine PS membrane and better antifouling performance [31].

Motivated with these aforementioned outstanding facts and in continuation of our endeavor to explore novel antimicrobial and anti-biofouling chitosan-based materials [26,32,33], we pursue in this work to design a facile protocol for surface-functionalization of chitosan by novel ionic liquid-based crosslinking agents; to fabricate poly(ionic) crosslinked chitosan Schiff bases (PICCSBs) which will be used as modulators for fine-tuning of the performance of PS-based membranes.

2. Materials and methods

Instrumentation; sources of materials; preparation of ionic liquid-based salicylaldehyde cross-linkers (**3a,b**), and low molecular weight chitosan (LMWC) are available in the electronic supplementary information (ESI†).

2.1. Synthesis of poly(ionic) cross-linked chitosan Schiff bases (PICCSBs)

Generally, a solution of ionic liquid-based salicylaldehydes cross-linkers (**3a,b**) (equivalent to half molar N-content in LMWCS) in EtOH (30 mL) was added to a solution of LMWC (2 g) in 200 mL of a mixed solvent system of 2% aqueous acetic acid/ethanol under vigorous stirring over a period of 30 min at 70 °C. After stirring for further 24 h at the same temperature, the solvent was partially evaporated under reduced pressure to give an oily residue which solidified by ultrasonic radiation in an excessive amount (300 mL) of ethyl acetate for 2 h. The isolated solids were collected by filtration and then washed with cold ethanol (3 × 10 mL). Finally, the desired products (**PICCSB$_{1,2}$**) were dried in a vacuum oven at 40 °C for 24 h. The obtained products were characterized as follows;

2.1.1. Poly-N,N-(5-(N′,N′-dimethylammonium)pyridinium dichloride)-bis-(salicylidene) chitosan) (PICCSB$_1$)

Yellow powder, yield (98%). FTIR (KBr, cm^{-1}): 3441 (vs, br), 3169 (m, br), 1652 (vs, sh), 1628 (vs, sh), 1520 (m, sh), 1349 (m, sh), 1275 (m, sh), 1156 (s, sh), 1059 (m, sh), 891 (m, sh), 744 (m, sh). ^{1}H NMR (600 MHz, $D_2O)_{60\ °C}$ δ (ppm): 11.15 (s, 2H), 8.81 (d, J = 6.5 Hz, 2H), 8.03–8.00 (m, 2H), 7.97 (dd, J = 6.5, 2.1 Hz, 2H), 7.84 (d, J = 2.4 Hz, 2H), 7.73 (dd, J = 8.7, 2.5 Hz, 2H), 7.34 (d, J = 8.7 Hz, 2H), 5.95 (s, 2H), 4.88 (s, 2H), 4.72 (s, 2H), 4.20–4.13 (m, 8H), 4.03 (d, J = 7.3 Hz, 2H), 3.98–3.74 (m, 12H), 3.44 (s, 4H), 2.97 (s, 6H), 2.35 (s, 6H).

2.1.2. Poly-N,N-(5-(N′,N′-dimethylammonium)pyridinium dichloride)-bis-(3-methylsalicylidene) chitosan) (PICCSB$_2$)

Canary yellow powder, yield (96%). FTIR (KBr, cm^{-1}): 3439 (vs, br), 3178 (m, br), 1650 (vs, sh), 1630 (vs, sh), 1522 (m, sh), 1356 (m, sh), 1276 (m, sh), 1157 (s, sh), 1063 (m, sh), 890 (m, sh), 749 (m, sh), and 556 cm^{-1}. ^{1}H NMR (600 MHz, 1% $CD_3COOD/D_2O)_{60\ °C}$ δ (ppm): $D_2O)_{60\ °C}$ δ (ppm): 11.15 (s, 2H), 8.83 (d, J = 6.5 Hz, 2H), 8.11–8.00 (m, 2H), 7.96 (dd, J = 6.7, 2.1 Hz, 2H), 7.83 (d, J = 2.5 Hz, 2H), 7.76 (dd, J = 8.6, 2.5 Hz, 2H), 5.92 (s, 2H), 4.85 (s, 2H), 4.72 (s, 2H), 4.25–4.13 (m, 8H), 4.03 (d, J = 7.3 Hz, 2H), 3.98–3.82 (m, 8H), 3.81–3.69 (m, 4H), 3.44 (s, 4H), 2.95 (s, 6H), 2.84 (s, 6H), 2.15 (s, 6H).

2.2. Preparation of pristine PS membrane (M_0)

The modified non-solvent induced phase inversion (NSIPI) technique was used to fabricate all membranes. In brief, a casting solution of PS was prepared by dissolving PS (3.8 g) in N-Methyl-2-pyrrolidone (NMP) (15.21 g, 15.66 mL) under vigorous stirring at 60 °C for 1 h. Then, this solution was de-aerated under vacuum for 15 min. Afterward, the bubble-free casting solution was molded by either spreading over a nonwoven polyester fabric (novatex2483) and immersion into a non-solvent phase (milli-Q water) at the room temperature. The membrane should be stored in for 3 days in milli-Q water to get rid of the residual NMP.

2.3. Fabrication of mixed-matrix membranes ($MMM_{1,2}$)

Generally, initially, homogenous solutions were prepared by dissolving PICCSBs (0.1 g) and PS (3.8 g), separately, in a mixed solvent system of 1% aqueous acetic acid/NMP (1:1 v/v, 10 mL) and NMP (9.20 g, 9.50 mL), respectively, by stirring (500 rpm) at 60 °C for 1 h. Then, the PICCSB solution was added in a very slow rate (1 drop/30 s) to the PS solution under vigorous stirring (1100 rpm) at 60 °C. An additional amount of NMP (0.93 mL) was added and the obtained turbid solution was vigorously stirred at 70 °C till obtaining a clear and homogeneous solution. Then, the casting solution was de-aerated under vacuum and molded using the NSIPI method as aforementioned. The compositions of all membranes are shown in Table 1.

2.4. Membrane physical characterization

Full details for the practical methods used for X-ray diffraction (XRD) analysis, determination of the porosity, hydrophilicity, swelling,

Table 1
Composition (wt%) of the prepared MMMs.[a]

Membrane ID	PS	NMP	AcOH	PICCSB$_1$	PICCSB$_2$
M_0	20.0	80.0	–	–	–
MMM_1	20.0	53.3	26.2	0.5	–
MMM_2	20.0	53.3	26.2	–	0.5

[a] PS, polysulfone; MMM, mixed-matrix membrane; NMP, *N*-methyl-2-pyrrolidone; AcOH, 1% acetic acid; PICCSB$_{1,2}$, poly(ionic) cross-linked chitosan Schiff bases.

and contact angles (Figs. S1 and S2, ESI†) of all membranes are described in the ESI†.

2.5. Membrane performance assessment

2.5.1. Pure water flux (PWF)

The PWF of each membrane with an effective surface area of 5 cm^2 was investigated using a lab-scale filtration apparatus (Fig. S3, ESI†) according to a protocol reported in our previous work [31]. The PWF (J_w) was calculated based on Eq. (1):

$$J_w = \left(\frac{Q}{A\Delta t}\right) \tag{1}$$

where Q = amount of pure water permeate through a MMM of area A (m^2) at time Δt (h) and J_w is expressed in L/m^2h.

2.5.2. Antifouling assessment

Bovine serum albumin (BSA) was chosen as a model protein to induce fouling to the surfaces of MMMs [34].

2.5.3. BSA ultrafiltration performance study

The fouling tendency of the membrane was assessed using the ultrafiltration experiment of an aqueous BSA solution through it. Initially, each MMM was compacted at a trans-membrane-pressure (TMP) of 0.1 MPa for 30 min. Then, the pressure on the membrane was raised to 0.3 MPa followed by filtration of pure water through the membrane. After 90 min of water flow, a steady-state water flux (J_{w1}) was calculated. Afterward, the pure water was replaced by an aqueous BSA solution (0.8 g/L), and the BSA flux (J_{BSA}) after 90 min flow was calculated. UV–Vis spectroscopy at 280 nm was used to monitor BSA rejection (R %) which was calculated according to Eq. (2):

$$R\% = \left(1 - \frac{C_{BSA}^{Permeate}}{C_{BSA}^{Feed}}\right) \times 100 \tag{2}$$

Here, $C_{BSA}^{Permeate}$ (mg/mL) and C_{BSA}^{Feed} (mg/mL) represent the BSA concentration in permeate and feed, respectively. After the BSA filtration experiment, the MMM was flushed with milli-Q water for 15 min before measuring the steady-state PWF again (J_{w2}). Finally, the antifouling capacity of the membrane was calculated in terms of flux recovery ratio (*FRR*) based on Eq. (3):

$$FRR\% = \left(\frac{J_{w2}}{J_{w1}}\right) \times 100 \tag{3}$$

The antifouling efficacies of membrane can be estimated from several parameters including *FRR*%, total fouling (R_t) ($R_t = 1 - J_{BSA}/J_{w1}$),

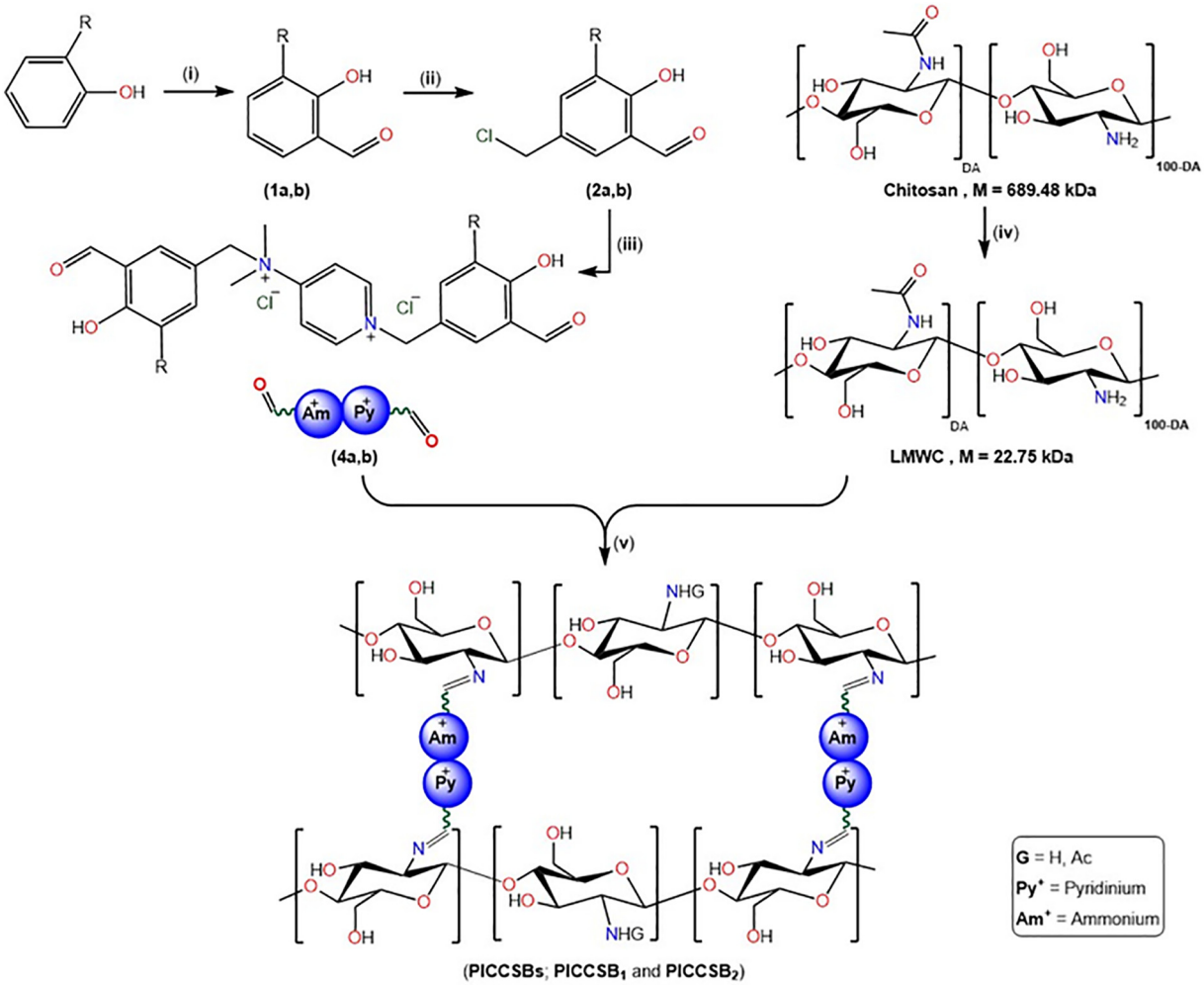

(i) $MgCl_2$, $(CH_2O)_n$, Et_3N, ACN, stir, r.t; HCl. (ii) CH_2O, $ZnCl_2$, HCl_{aq}, HCl_g, stir, r.t.; (iii) DMAP, toluene, stir, 80 °C, N_2; (iv) 1% CH_3COOH, 30% H_2O_2 stir, r.t.; (v) EtOH, stir, 70 °C.

Scheme 1. Schematic flowchart of different chemical reactions used for the preparation of ammonium-pyridinium-based TSILs (crosslinking agents) (**3a,b**) and poly(ionic) crosslinked chitosan Schiff bases (PICCSBs; $PICCSB_1$ and $PICCSB_2$).

Table 2
M_{av}, DD%, and DC% of LMWCS and PECSBs.

Sample	M_{av} (KDa)	DD (%)			EA calcd (found) (%)			DC (%)
		Titration	FTIR	EA	C	H	N	
LMWC	12.75	87.63	85.69	88.60	45.06 (44.93)	6.82 (6.87)	8.45 (8.42)	– –
$PICCSB_1$	–	–	–	–	50.57 (50.44)	6.23 (6.27)	7.94 (7.85)	35.85
$PICCSB_2$	–	–	–	–	50.78 (50.63)	6.41 (6.45)	7.84 (7.71)	31.75

reversible fouling (F_r) ($F_r = (J_{w2} - J_{BSA}) / J_{w1}$), and irreversible fouling (F_{ir}) ($F_{ir} = (J_{w1} - J_{w2}) / J_{w1}$) [35].

3. Results and discussion

3.1. Chemistry of synthesis of PICCSBs ($PICCSB_1$ and $PICCSB_2$)

New task-specific ionic liquids (TSILs) bearing ammonium and pyridinium cations have been fabricated starting from salicylaldehyde derivatives (3-R-Sal; R = H, Me) using a simple and common synthesis route that involves chloromethylation process to afford the chloromethyl salicylaldehyde derivatives (**2a,b**) which were used for the quaternization of 4-dimethylaminopyridin (DMAP) to yield dual ammonium-pyridinium-based TSILs (**3a,b**) (See Scheme 1). These TSILs were applied as crosslinking agents for the as-prepared low molecular weight chitosan (LMWC) through Schiff base condensation reactions to prepare poly(ionic) crosslinked chitosan Schiff bases (PICCSBs; $PICCSB_1$ and $PICCSB_2$). These new antifouling agents were obtained in excellent yields (96–98%) and fully characterized (structurally and morphologically) based on elemental, spectral, and scanning electron microscopy (SEM) analysis.

3.2. Structural characterizations of LMWC and PICCSBs

3.2.1. Average molecular weight (M_{av}), degree of deacetylation (DD), and degree of cross-linking (DC)

The average molecular weight (M_{av}) for the LMWC sample was calculated from the intrinsic viscosity [η] values of its solution in CH_3COOH (0.3 mol/L) containing CH_3COONa (0.2 mol/L) according to the Mark–Houwink–Sakurada (MHS) Eq. (3) [36]:

$$[\eta] = K\,(M_{av})^{\alpha} \quad (3)$$

where η is the intrinsic viscosity; K and α are viscometric constants, $K = 0.93$ (mL/g) and $\alpha = 0.76$. The average molecular weight for LMWC samples was found to be 12.75 KDa.

Three different techniques (volumetric titration, FTIR, and elemental analysis (EA)) have been used for the calculation of the DD% for LMWC (see ESI†). The obtained results were collected in Table 2.

As the extent of crosslinking of LMWC with new TSILs is strongly correlated to the content of amino groups on the surface of LMWC, thus, the degree of crosslinking (DC) can be easily investigated through determining the amount of free amino groups on the surface of LMWC sample before and after crosslinking, using volumetric titration (see ESI†). Again, the obtained results were collected in Table 2.

3.2.2. Fourier-transform infrared spectroscopy (FTIR)

FTIR technique offers preliminary spectral evidence for the successful conversion of LMWC into PICCSBs. Comparing the FTIR spectra of the PICCSBs with the LMWC spectrum (Fig. 1A) revealed the retention of the main peaks that are characteristic for the LMWC backbone (3440 cm^{-1}, O-H and N-H; 1650 cm^{-1}, amide I C=O; 890 cm^{-1}, glycosidic bond) [26,37], in the spectra of PICCSBs; confirming sustain the LMWC skeleton even after its surface modification.

In addition, the emergence of new absorption bands in the FTIR spectra of the PICCSBs around 1630 and 1275 cm^{-1}, characteristic for azomethine (H–C=N) and aryl–O fragments, respectively, of the salicylidene segment; proves the success of crosslinking of LMWC chains through Schiff base condensation between the amino and carbonyl groups of chitosan chains and ionic liquid-based salicylaldehyde crosslinkers, respectively. In addition, the observation of three predominant peaks (1520 cm^{-1}, C=N; 749 cm^{-1}, Py ring; and 556 cm^{-1}, Het-N^+Cl^-), distinctive for the pyridinium-ammonium ionic liquid terminal [26], confirm the spreading of ionic liquid compartments on the surface of poly(ionic) cross-linked chitosan Schiff bases (PICCSBs).

3.2.3. NMR spectroscopy

The coexistence of major NMR peaks characteristic for the ammonium-pyridinium-based crosslinking agent (**3a**) and LMWC in the ^1H NMR spectrum of poly(ionic) crosslinked chitosan Schiff base ($PICCSB_1$) (Fig. 2) confirms its successful formation. As shown in Fig. 2, two sets of ^1H signals were observed. The first group (framed with black rectangles) was noticed at chemical shift values 5.12,

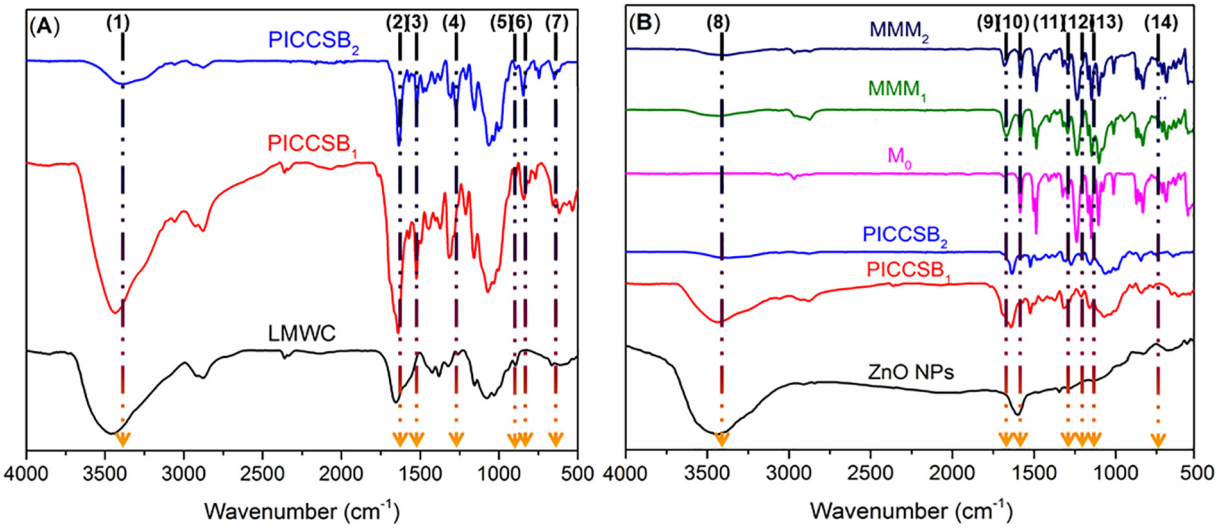

Fig. 1. Collective FTIR spectra of: (A) low molecular weight chitosan (LMWC) and poly(ionic) cross-linked chitosan Schiff bases (PICCSBs); (B) PECSBs ($PICCSB_{1,2}$), native polysulfone (PS) membrane (M_0), and mixed-matrix membranes ($MMM_{1,2}$) for comparison of their respective characteristic vibration bands. (**1**), (**8**) for NH.

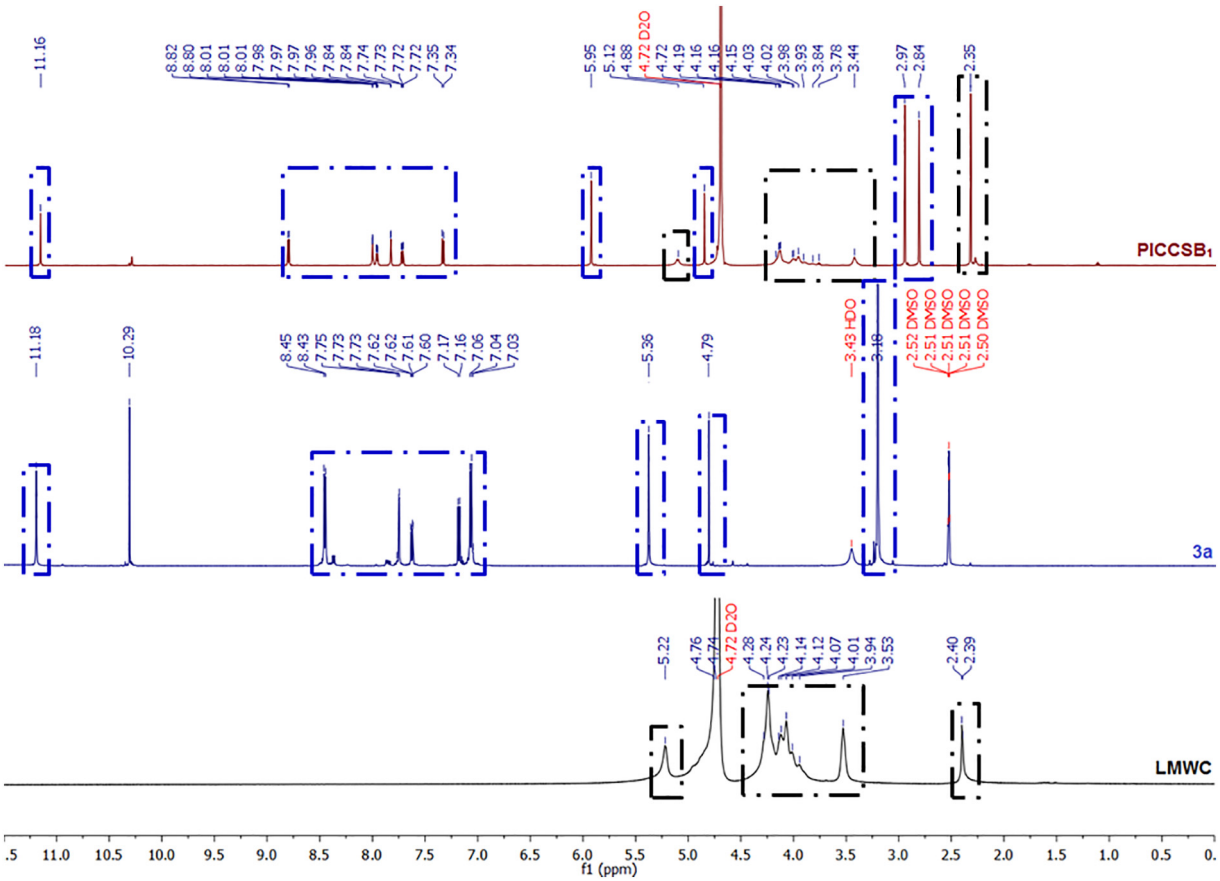

Fig. 2. ^{1}H NMR spectra of LMWC, ammonium-pyridinium-based crosslinker (**3a**), and poly(Ionic) crosslinked chitosan Schiff base (PICCSB$_1$) solutions in D_2O, DMSO, and D_2O, respectively, at 200 MHz. Peaks framed with black rectangles are characteristic for LMWC backbone protons. While the other framed with blue rectangles are distinctive for crosslinking agent (**3a**).

4.19–3.44, and 2.35 ppm, are assignable to resonances of anomeric protons, H3–H6 connected to the non-anomeric carbons (C3–C6) in the glucopyranose ring, and acetyl H atoms (GlcNAc) in the chitosan backbone [26,38]. While the other set of peaks (framed with blue rectangles), distinctive for cross-linking agent (**3a**), was centered at δ (ppm); 11.16 (phenolic OH), 8.82–7.34 (azomethinic and aromatic protons), 5.95 (methylene H atoms), 4.88, 2.97, and 2.84 (different methyl H atoms). Furthermore, the disappearance of aldehyde proton signals in the spectrum of PICCSB$_1$ (centered at 10.29 ppm in the spectrum of **3a**), coupled with the great diminishing in the intensity of the peak characteristic for amino group (centered at 5.22 ppm in LMWC spectrum); confirms the formation of PICCSB$_1$ by partial Schiff base condensation of aldehyde and amino groups of crosslinker (**3a**) and LMWC, respectively. Moreover, the ^{13}C NMR spectrum of PICCSB$_1$ emphasize the successful crosslinking of LMWC chains by ammonium-pyridinium-based crosslinker (**3a**) through Schiff base condensation reaction, as revealed from the emergence of new low-field peaks at 160.72, 160.62, and 154.87 ppm attributable for the resonance of azomethinic and phenolic carbon-atoms, respectively, of salicylidene backbone.

3.2.4. Morphological characterizations of PICCSBs

The SEM micrographs (Fig. S4, ESI†) were used to investigate the changes in the surface morphologies of PICCSBs in comparison to that of the native LMWC. As evident in Fig. S3, there are significant differences between the surface morphologies of PICCSBs and LMWCS. LMWCS displays a dense, smooth, and flat surface, while; PICCSBs show woven-like or sponge-like surfaces. This may be ascribed to the formation of additional hydrophilic (ionic charges, phenolic, and imine linkages) and hydrophobic sites (benzene rings) on the surfaces of PICCSBs that enhanced the interactions between LMWC chains in PICCSBs through H-bonding and hydrophobic interactions resulting in the formation of surfaces with cross-sectional pores and micro-void network.

3.3. Membranes characterization

3.3.1. Attenuated total reflection (ATR)-FTIR

Comparing the ATR-FTIR spectra of the as-fabricated MMMs (MMM$_{1,2}$) with that of native PS membrane (M$_0$) (Fig. 1B) offers preliminary evidence for the incorporation of PICCSBs into the matrix of polysulfone, confirming the successful fabrication of MMMs. To name few, as compared to the spectrum of M$_0$, it is noticed that new spectral peaks were observed in the spectra of MMMs around 3450, 1660, 1579, 1281, and 858 cm^{-1} which can assignable for the vibrations of N-H and O-H, azomethine (H-C=N), C=N, Ar–O, and $R_4N^+Cl^-$ that belong to the chitosan, salicylidene, and ionic liquid segments of PICCSBs [30,31]. Moreover, the asymmetric and symmetric stretching vibration peaks of the O=S=O, that distinctive for PS backbone, were observed at *ca* 1295 and 1149 cm^{-1}, confirming the reserving of the structural features of PS after its surface modification with PICCSBs.

3.3.2. Morphology of the membranes

The thicknesses of new MMMs were measured using a micrometer screw gauge and were in the range of 98–115 μm. In addition, their surface and cross-section morphologies were inspected by SEM technique (Figs. 3 and S5, ESI†). Generally, the overall porosity of the membrane surface has significantly increased upon incorporation of PICCSBs into the matrix of PS, as shown in Fig. 3A–C. The surface of the native PS membrane (M$_0$) is smooth and dense with a non-porous texture (Fig. 3A). Whereas, the surfaces of MMM$_1$ and MMM$_2$ are almost homogeneous porous networks with pore diameters (PD) in the ranges of 0.7–1.1 and 0.5–0.8 μm, respectively (Fig. 3B,C). On the other hand, it

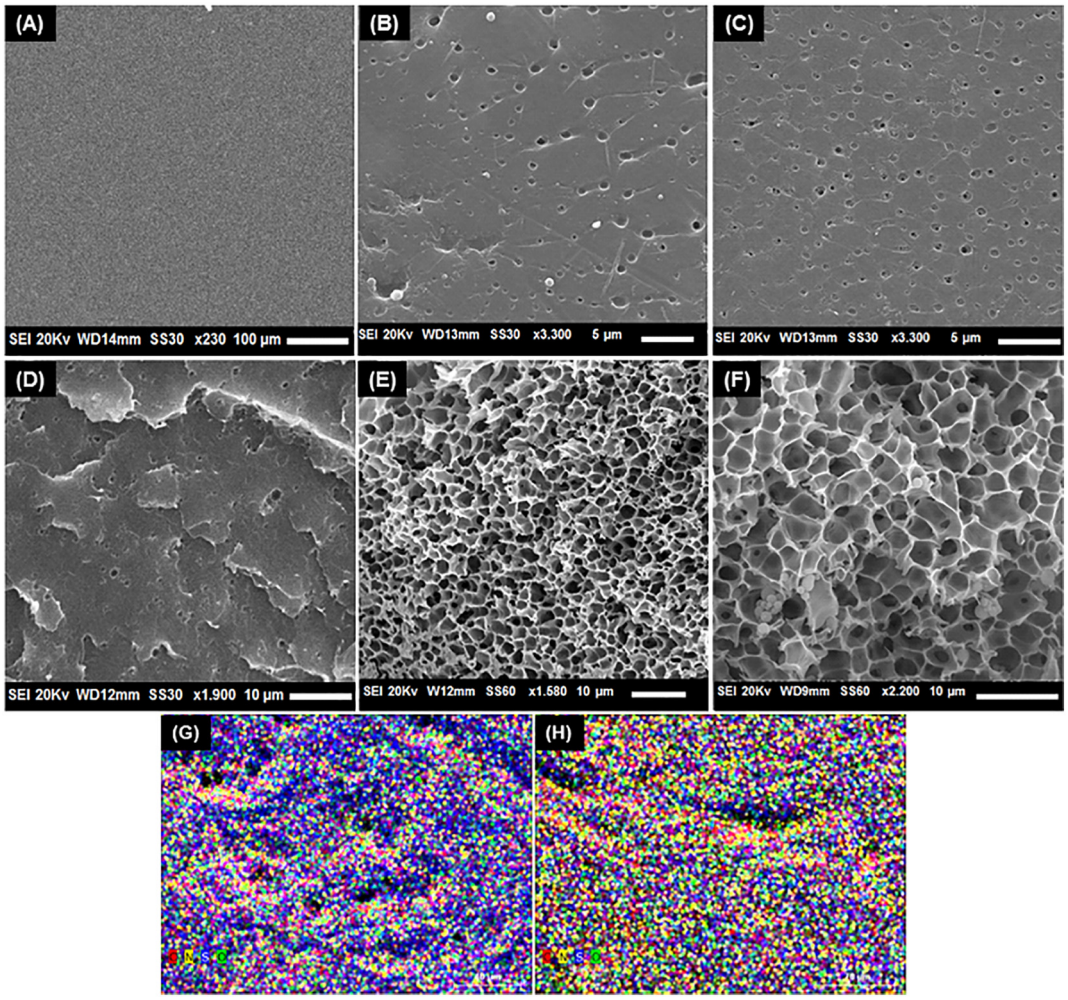

Fig. 3. Surface and cross-sectional SEM micrographs of: (A, D) M_0 (PS); (B, E) MMM_1 (PS-PICCSB$_1$); and (C, F) MMM_2 (PS-PICCSB$_2$). (G, H) The EDX elements (C, N, S, O) mapping images of MMM_1 and MMM_2, respectively; illustrating the atomic composition of new membranes.

is evident from the cross-sectional SEM micrographs (Fig. 3D–F) that both MMMs exhibited asymmetric extremely porous micro-void structures with many grooves and chancels on their respective upper layers (Fig. 3E,F), as compared with the parent PS membrane which has a layered structure with very few pores (Fig. 3D). Noteworthy, MMM_1 has larger pores (diameters range 2.4–3.5 μm) than those in MMM_2 (diameters range 1.1–1.5 μm). The significant enhancement in the membrane porosity upon the incorporation of PICCSBs could be ascribed to their extremely hydrophilic nature that enhances the overall hydrophilicity of the membrane to a great extent. This superior hydrophilicity has promoted the mutual diffusion of the membrane components from the casting solvent (NMP) to the non-solvent phase (coagulation solvent, water), and thus the coagulation time for the membrane will increases. Consequently, this slow coagulation allows longer phase inversion time coupled with a lower rate of segregation of PICCSB from casting medium up to the NMP-water interface, promoting the self-induced pore growth [31]. Interestingly, all new MMMs are typical ultrafiltration (UF) membranes with macro-pores upon the surface (PD 0.5–1.1 μm) and macro-voids (diameters range 1.1–3.5 μm) embedded across the membrane network.

The elemental composition of the MMMs was inspected using energy-dispersive X-ray (EDX) technique. The obtained results were represented as element mapping images (Fig. 3G,H) and EDX spectra (Figs. S6–S9, ESI†). The EDX element mapping results demonstrated the distribution of PICCSBs on the surface of PS. As the carbon, oxygen, and sulfur elements already exist in the PS surface, the element mapping of nitrogen and chlorine elements (from PICCSBs) was chosen to distinguish between the native PS membrane and MMMs. As shown in (Fig. 3G,H) and (Fig. S5), the nitrogen and chlorine elements can be detected only on the surface of MMMs.

3.3.3. Water uptake (hydration), contact angle and porosity measurements

The hydrophilicity of new membranes was assessed based on their respective water-contact angle (WCA) and water uptake (i.e. hydration) values. The WCA of the MMMs was decreased from 85.92° (M_0) to 45.73° (MMM_1) by adding PICCSB$_1$ into the matrix of PS membrane (Fig. 4B). This can be attributed to the superior hydrophilic nature of PICCSB$_1$ owing to the strong hydration effect of pyridinium and quaternary ammonium groups [39,40]. Noteworthy, MMM_1 displayed a lower contact angle (WCA = 45.70°) than MMM_2 (WCA = 50.11°), indicating that MMM_2 has lower hydrophilic characters than MMM_1. This may be ascribed to the presence of hydrophobic methyl groups in the crosslinker of PICCSB$_2$ (incorporated in MMM_2) which reduce its overall hydrophilicity and consequently its respective blend membrane (MMM_2), as well. Additionally, as evident in Fig. 4A, the water uptake (WU) of the MMMs was sharply increased from 27.23% (M_0) to 95.31% (MMM_1) and 87.22% (MMM_2) after incorporation of PICCSB$_1$ and PICCSB$_2$, respectively, into the matrix of M_0. Generally, the incorporation of PICCSBs into the matrix of the PS has improved its hydrophilicity to a great extent. Noteworthy, WU performance is pH-dependent with maximum uptake from the acidic medium. For instance, MMM_1 showed WU values; 95.3%, (pH 4), 89.84% (pH 7), and 83.73% (pH 9).

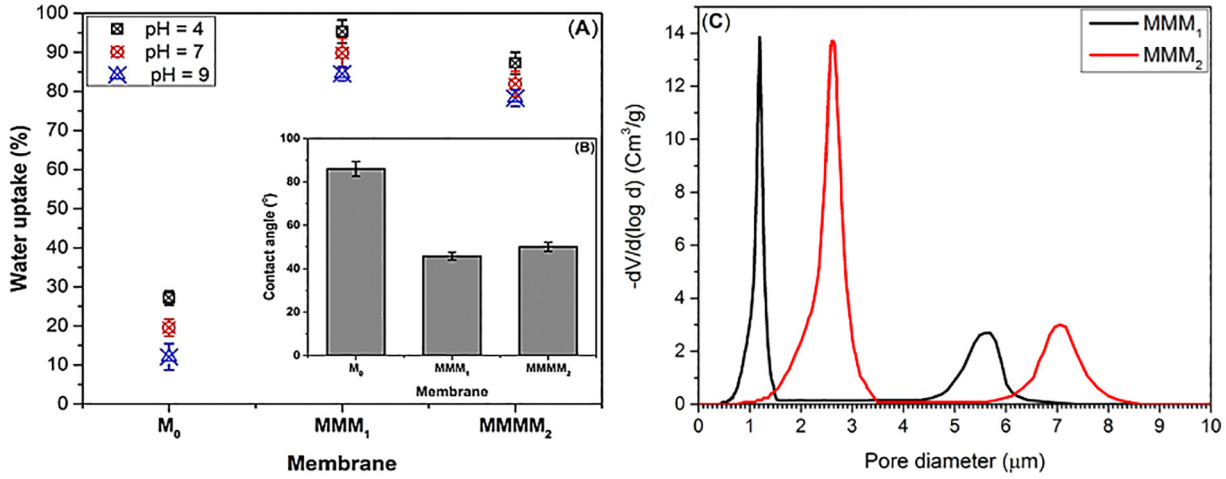

Fig. 4. (A) The pH-dependent water uptake (hydration) of MMMs as compared to the neat PS membrane (M_0). (B) Water contact angles (WCA) of new MMMs in comparison with M_0. (C) Pore size distribution (PSD) curves of MMM_1 and MMM_2.

This may be attributed to the protonation of the unreacted amino and phenolic groups of PICCSBs at lower pH 4, increasing the hydration effects of these fragments.

As the performance of any membrane is strongly correlated with the pore size distribution (PSD) on the internal and external surfaces of the membrane, therefore, the PSD of new MMMs was investigated using A QUANTACHROME POREMASTER 60-GT, as shown in Fig. 4C. As evident in this figure and in Fig. S4, ESI†, both membranes ($MMM_{1,2}$) exhibited many channels and pores. The surface of each membrane shows many channels with internal diameters in the ranges of 4.5–6.8 μm (MMM_1) and 5.6–8.5 μm (MMM_2). On the other hand, the core of each membrane involves many spherical and polygonal pores with a hierarchical pore size distribution ranging from small internal pores with PD values (MMM_1, 0.7–1.3; MMM_2, 1.3–3.7 μm) to large internal pores with PD values (MMM_1, 57.5–77.4; MMM_2, 76.3–104.5 μm).

3.4. Membranes performance

3.4.1. Zeta potential and ion-exchange capacity studies

The outer surface charge of native and mixed-matrix PS membranes was investigated using zeta (ζ) potential measurements. As evident from Fig. 5A, the native PS membrane displayed a very low positive ζ-potential at pH 4, whereas, it is exhibited a negative potential at pH > 4 (isoelectric pH (pl-pH) = 4.25). Therefore, the cationic additives (PICCSBs) could be readily deposited on the negatively-charged outer surface of PS to fabricate mixed-matrix PS membranes (MMMs). This leads to the acquisition of positive charges on the outer surfaces of these MMMs and consequently positive ζ-potentials. These positive values for ζ-potentials for MMMs were observed over a broad pH range (4–8) and are attributed to the spreading of quaternary ammonium and pyridinium groups onto the barrier interface of membranes, preventing the absorption of anions onto their surfaces in acidic medium [41]. Interestingly, the ζ-potentials of the MMM surfaces decreased systematically with an increase of pH of the medium. Moreover, at higher pH values (pH > 8.25) the ζ-potentials for these membranes became negatively charged. For instance, the ζ-potential of MMM_1 has decreased from +51.2 mV (pH 4) to +8.1 mV (pH 6) and −9.0 (pH 9). These changes may be ascribed to the slight accumulation of anions (OH^-, from the alkaline medium; Cl^- from quaternary salt) on the surface of the membranes, diminishing their streaming potentials [42,43]. In addition, the deprotonation of salicylidene fragments in PICCSBs under pH > 6, forming phenolate anions [44], may also share in the dramatic decrease of the positive surface potentials to reach negative values at pH > 8, eventually. The isoelectric pH (pl-pH) values were found to be 8.25 and 8.26 for MMM_1 and MMM_2, respectively. Overall, these results confirm that the incorporation of PICCSBs into the matrix of the PS membrane imparts persistent positive charges onto its outer surface over a wide pH range.

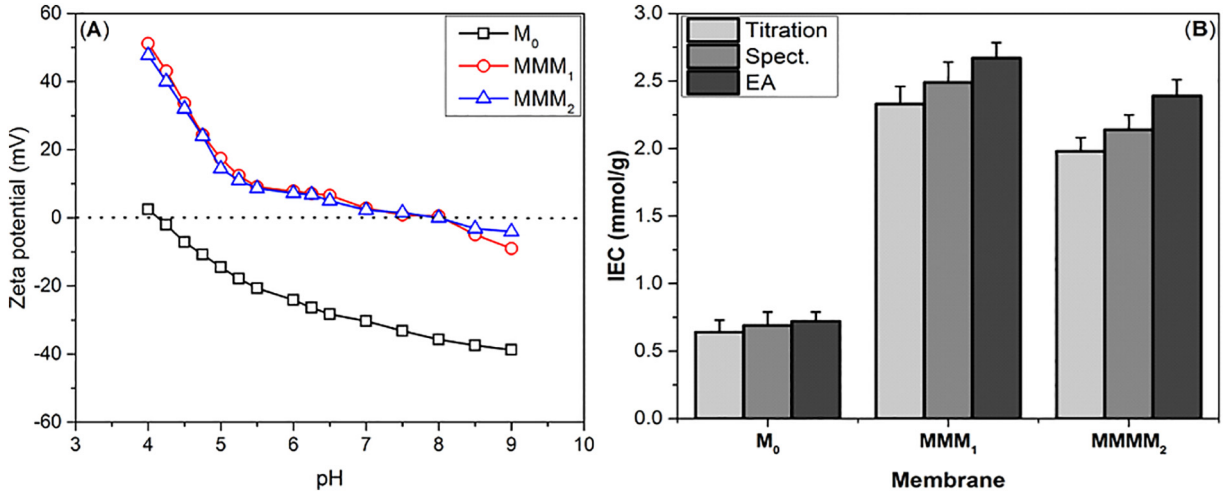

Fig. 5. (A) Zeta-potentials of native (M_0) and mixed-matrix PS membranes (MMM_1, MMM_2) at pH 4–9. (B) The ion-exchange capacity (IEC) of M_0, MMM_1, and MMM_2 using three different determination methods (EA, elemental analysis; titration, indirect determination of nitrate by titration of liberated Cl^- ions using Mohr's method; Spect., spectrophotometric).

The ion-exchange capacity (IEC) is a crucial feature for assessing the selectivity of membranes. Therefore, three different techniques were applied to determine the IEC of the nascent PS membrane (M_0) and the new MMMs towards the nitrate anion (mimic to denitrification process); namely, elemental analysis (EA) (N%) and indirect titration or spectrophotometric determination of the NO_3^- anion as represented in Fig. 5B. In general, blending of PICCSBs into PS membrane has greatly improved its anion-exchange capacity owing to spreading of active cationic sites (ammonium and pyridinium) on the surface of MMMs.

The theoretical (virtual) IEC values were calculated from the EA results using Eq. (4) [45];

$$\mathrm{IEC} = 10\,\frac{X_N}{M_N}\ \mathrm{mmol\ g^{-1}} \tag{4}$$

where, X_N and M_N represent the weight fraction of nitrogen (%) in the membrane, after NO_3^- uptake, and its molar mass (g mol^{-1}), respectively. Based on N% in each membrane and Eq. (4), the IEC values of membranes M_0, MMM_1, and MMM_2 were 0.64 ± 0.09, 2.33 ± 0.13, and 1.98 ± 0.11, respectively. However, the IEC calculated for the MMMs from EA are 6% ± 1% lower than that measured spectrophotometrically, whereas, they are 15% ± 2% lower than that obtained by titration. This discrepancy mainly arises from the existence of free basic amino groups, due to PICCSBs blending, in the network of membranes [45]. These amine groups would surely affect the titration and spectrophotometric determination of the nitrate anion.

Generally, the different methods used for IEC determination show that the nitrate-exchange capacity of the $PICCSB_1$-incorporated membrane (MMM_1) is ~14% higher than that of the $PICCSB_2$-supported membrane (MMM_2). This preferable nitrate-uptake by MMM_1 could be attributed to the higher population of active cationic moieties (anion-selective groups) on its surface in comparison to MMM_2; as revealed from the elevated values of N% content, DC%, and positive surface charge (ζ-potential) for MMM_1 (cf. Table 2, Fig. 5A). Interestingly, the nitrate-exchange capacity for our new membrane (MMM_1) was 3.4-times higher than that reported for the most efficient quaternary ammonium polysulfone (QAPS) membrane [46] and 1.3-folds higher than that for the UF microreactor (MMR) [47].

3.4.2. Permeation properties

The effect of incorporation of PICCSBs into PS membrane upon its permeation performance was studied by filtration of pure water and protein (bovine serum albumin, BSA) solution, separately, through the pristine PS membrane (M_0) and MMMs; to investigate the pure water flux (PWF) and BSA rejection for each membrane. From Fig. 5A it is evident that the pristine PS membrane shows very low permeability for both pure water and BSA solution as revealed from its ultra-declined PWF (25.82 L/m^2 h) and raised BSA rejection (98.6%). This could be attributed to the high hydrophobicity coupled with the presence of a dense non-porous layer on the outer surface of M_0 membrane; making it inconvenient for most practical UF applications. Notably, the permeability of the UF membranes can be controlled by fine-tuning of their surface hydrophilicity, overall porosity, and operating conditions [31]. In this scenario, this study employed the new strongly hydrophilic agents (poly(ionic) crosslinked chitosan Schiff bases (PICCSBs)) as synergistic hydrophilicity-modulators, antifouling, and pore-forming/stabilizing additives for a PS ultrafiltration membrane. The overall permeability of the PS membrane was greatly boosted after blending with the hydrophilic additives (PICCSBs) to fabricate the new MMMs. For instance, the $PICCSB_1$-supported membrane (MMM_1) can achieve a PWF of 238.61 L/m^2 h which is 9.3-times higher than that of the neat PS membrane (M_0), whereas, the protein retention by MMM_1 was only 41.9%, (2.5-fold lower than that of the M_0). On the other hand, the PWF and protein rejection for the MMM_2 membrane was 222.43 L/m^2 h and 47.6%, respectively.

This amazing water permeation performance could be ascribed to the greatly enhanced surface hydrophilicity and porosity of PS owing to PICCSBs blending. Moreover, these hydrophilic additives (PICCSBs) will also enhance the interaction between the hydrophilic pores and pure water within the porous framework of MMMs; resulting in improved water mass transfer across them. Contrary, PICCSBs will diminish the hydrophobicity of membranes resulting in reducing their propensity to adsorb the organic contaminants (BSA) [46].

3.4.3. Antifouling performance

The antifouling performance of newly fabricated mixed-matrix membranes (MMM_1, MMM_2) was investigated as compared to the neat PS membrane (M_0) using three consecutive ultrafiltration experiments (pure water-BSA solution (0.5 g/L)- pure water water) through each membrane under fixed operation conditions (P, 0.3 MPa; T, 26 °C). As depicted in Fig. 6B, the PWF of M_0 was remarkably decreased upon exchanging the pure water (phase I, Fig. 6B) with a fouling-inducing protein (BSA) solution (phase II, Fig. 6B). This drop is attributed to the hydrophobic nature of the neat PS surface which enhances mutual interactions between M_0 and BSA and increases the membrane fouling propensity to form a hydrophobic water-impermeable interface (M_0-BSA) on the membrane surface. Thus, the native PS membrane demonstrated a very low flux recovery ratio (FRR) (37%, Fig. 7). In

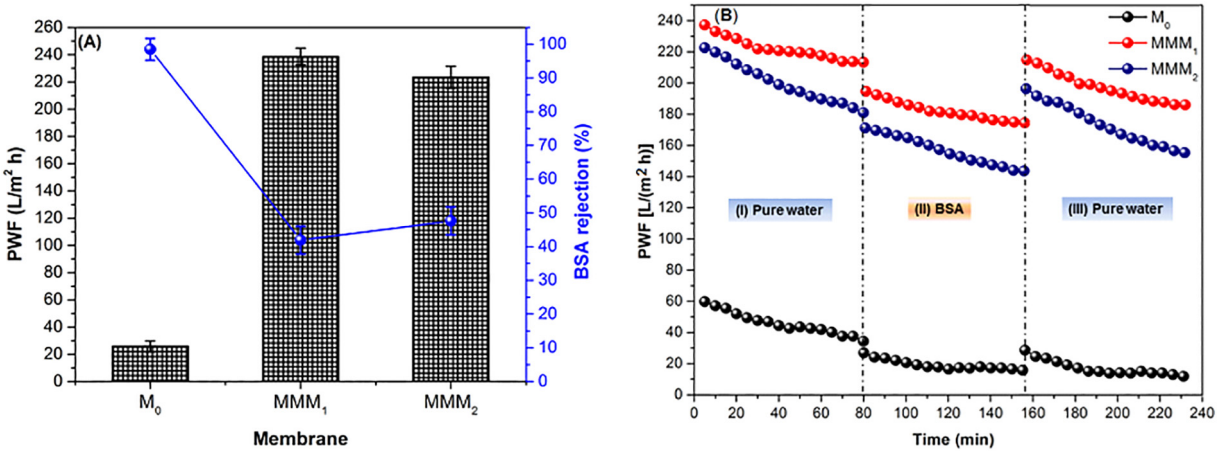

Fig. 6. (A) Comparison of the pure water flux (PWF) and BSA rejection of the pristine PS membrane (M_0) and MMMs (MMM_1, MMM_2). Measuring conditions: (i) PWF; 5 cm^2 membrane, milli-Q water, trans-membrane-pressure (TMP) 0.10 MPa/30 min, operating pressure (OP) 0.3 MPa, 26 °C, 90 min experimental duration time; (iii) BSA rejection; 5 cm^2 membrane, 0.5 g/L BSA solution, TMP 0.10 MPa/30 min, OP 0.3 MPa, 26 °C, 90 min experimental duration time. (B) Time-dependent fluxes of the different PS-based membranes during three consecutive cycles of milli-Q water, BSA, and milli-Q water ultrafiltration at 0.3 MPa and 26 °C.

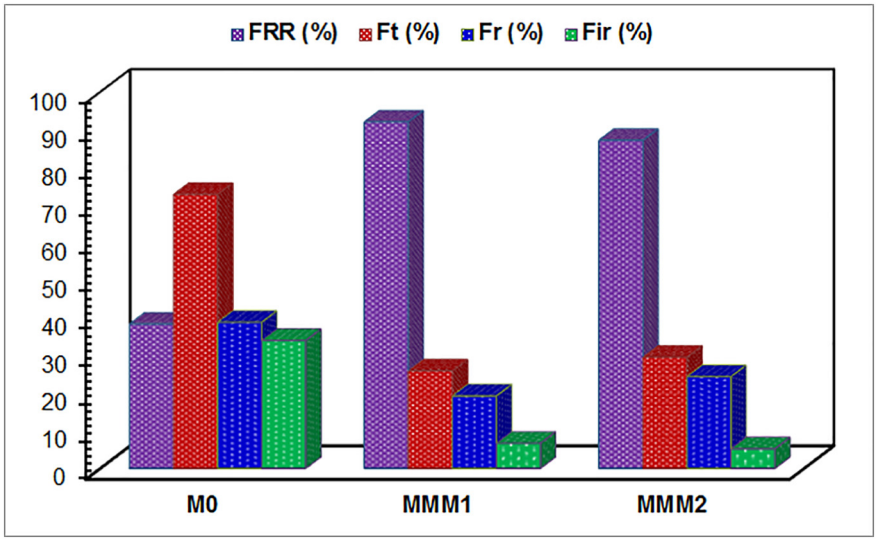

Fig. 7. Results of fouling parameters; flux recovery ratio (FRR), total fouling (F_t), reversible fouling (F_r), and irreversible fouling (F_{ir}) for the native PS membrane(M_0) and mixed-matrix membranes (MMM_1, $MMMM_2$).

contrast, PICCSBs-supported PS membranes (MMM_1, MMM_2) present high permeability before, during, and after BSA ultrafiltration with elevated FRR% than that assigned for bare PS membrane. For instance, $PICCSB_1$-PS membrane shows the highest permeability during all ultrafiltration stages (I - III) with little flux declining degree after filtration of the foulant solution (BSA) and a highest FRR% (91%, Fig. 7). Again, this can be attributed to the increase of the surface and pore hydrophilicity of MMM_1, owing to the incorporation of $PICCSB_1$, which reduces mutual interactions between MMM_1 surface and BSA, reducing its fouling propensity, accordingly.

As aforesaid, that the FRR is a key parameter in predicting the membrane fouling resistance, moreover, the results of fouling indices (total (F_t), reversible (F_r), and irreversible (F_{ir}) fouling) are important in providing more detail concerning the fouling propensity and mechanism. In general, the FRR results (Fig. 7) proved that the incorporation of PICCSBs into PS matrix has remarkably improved its antifouling performance. The values of FRR for the bare, $PICCSB_1$-, and $PICCSB_2$-supported PS membranes (M_0, MMM_1, MMM_2) were 39.1, 91.9, and 87.1%, respectively; indicating the superior fouling impedance of the PICCSBs-blended membranes. Interestingly, the trend of FRR changes is in accordance with the results of WCA and PWF of the as-fabricated MMMs. The excellent fouling resistance of MMMs can be ascribed to the adsorption of water molecules over the hydrophilic surface of the membrane to form a thin hydration layer of water molecules upon the outer membrane surface that blocks the adsorption of organic foulants [48].

The fouling indices depicted in Fig. 7 revealed that the values of total, reversible, and irreversible fouling for all mixed-matrix membranes were less than that of bare PS membrane. For example, values of F_t, F_r, F_{ir} were decreased from 72.25, 38.78, and 33.95% for the native PS membrane (M_0) to 25.88, 19.23 and 6.64%, respectively, for the most fouling-resistant membrane (MMM_1). Notably the reversible fouling is due to the reversible adsorption-desorption processes of foulant molecules and the latter can be easily removed by a simple hydraulic cleaning (water flushing), whereas, the irreversible fouling arises from the stable adsorption of foulant molecules on the surface and/or pores of the membrane and can be only removed by chemical processes. Once more, the better antifouling features of the PICCSBs-PS membranes over the native PS membrane can be explained by increased hydrophilicity of the modified membranes. The integration of PICCSBs into the membrane matrix imparted many accessible H-bond donor/acceptor sites (hydroxyl, carbonyl, amino, and azomethine groups) for the surface of the PICCSBs-supported membranes, inducing the formation of a thin hydration layer of water film by H-bonding interactions on the surface of PS membrane. This hydration layer prevents the adsorption of fouling-inducing molecules on the membrane surface and the subsequent fouling process, accordingly [48]. In brief, the potent hydrophilic additives (PICCSBs) have the capacity to form a hydration barrier that helps in reducing the adsorption of fouling-inducing molecules (BSA) on the membrane surface, minimizing membrane fouling. The results of fouling parameters have confirmed earlier results obtained from measurements of water contact angle and pure water flux.

Eventually, it would be interesting to compare our results with those previously reported in the literature as depicted in Table 3 [32,49–51]. Our membranes (MMM_1 and MMM_1) were more hydrophilic, as revealed from elevation of water contact angle (WCA) values, and consequently have greater water uptake (WU) than most reported PSF-based membranes. This in turn leads to higher pure water throughput along with low fouling propensity [31]. Where, MMM_1 displayed very high pure water permeability, in comparison to other MMMs, as revealed from the elevated PWF values.

In addition, the decreasing in fouling indices, such as diminished BSA-rejection values coupled with higher flux recovery ratio (FRR), is

Table 3
Comparison of the physical parameters and performance indices of our as-fabricated membranes with those previously reported in the literature[a].

Membrane	WCA (°)	WU (%)	PWF (L/m^2 h)	BSA-R (%)	FRR (%)	Ref.
CS@PSF	79.2	67.2	76.215	68.2	73.1	[31]
PILCSB@PS	76.4	75.1	129.17	43.1	87.2	[31]
PILCSB@TNP@PS	68.4	83.5	158.10	36.9	88.6	[31]
CS@CNTs@PS	63.5	–	55.34	–	–	[49]
CS/CNTsCOOH/PS	53.4	–	63.76	–	–	[49]
NSCS@PS	68.3	–	117.09	–	70.8	[50]
NPPCS@PS	66.8	–	118.53	–	75.7	[50]
QAPS	65.2	56.8	88.34	52.5	78.5	[51]
GO@QAPS	57.5	64.2	150.11	42.4	89.2	[51]
MMM_1	45.7	95.3	238.61	41.9	91.9	Our work
MMM_2	50.1	87.2	222.43	47.6	87.1	Our work

[a] WCA, water contact angle; WU, water uptake; PWF, pure water flux; BSA-R, bovine serum albumin rejection; FRR, flux recovery ratio; PILCSB, poly-ionic liquid chitosan Schiff base; TNP, titanium oxide nanoparticles; CNTs, multiwall carbon nanotubes; CNTsCOOH, Carboxy functionalized carbon nanotubes; NSCS, N-succinyl chitosan; NPPCS, N-propylphosphonyl chitosan; QAPS, Quaternized ammonium polysulfone; GO, graphene oxide.

indicative for the extremely low fouling propensity of our as-fabricated membranes, as compared to the reported ones. In general, the new fabricated membranes in this work could be ranked in the forefront of PSF-based membranes in comparison to the earlier reported ones, and may offer promising ultrafiltration membranes for nitrate-polluted water remediation.

4. Conclusion

New poly(ionic) cross-linked chitosan Schiff bases (PICCSBs) have been successfully synthesized using a facile and straightforward chemical protocol. PICCSBs have been used to improve the main characteristics of PS membrane including hydrophilicity, porosity, permeability, and fouling-resistance, as well as, nitrate uptake. The positively-charged PS-PICCSBs mixed-matrix membranes (MMMs) were fabricated by the nonsolvent-induced phase separation (NIPS) technique. The results of elemental and spectral analysis as well as SEM-EDX examination confirm the successful fabrication of PICCSBs and MMMs. In general, the main properties of PS membrane (porosity, hydrophilicity, surface charge, and fouling-resistance) have been positively affected and greatly improved after blending with PICCSBs, compared to the native PS membrane. From SEM images it is evident that the new MMMs are typical ultrafiltration (UF) membranes with macro-pores spread over their surfaces with a pore diameter (PD) range 0.5–1.1 μm and macro-voids (PD range 1.1–3.5 μm) embedded into the membrane network. The water contact angle (WCA) has declined from 85.92° (M_0) to 45.72° (MMM_1) and 50.11° (MMM_2); indicating increased hydrophilicity of the PICCSBs-supported membranes. Simultaneously, the water uptake (WU) of the MMMs was sharply increased from 27.23% (M_0) to 95.31% (MMM_1) and 87.22% (MMM_2) after incorporation of $PICCSB_1$ and $PICCSB_2$, respectively, into the matrix of M_0. The PS membrane surface potential has switched from negative to positive values, over a broad pH range (4–8), by blending with PICCSBs as revealed from the measured zeta potentials. The pure water flux (PWF) values of PICCSBs-blended membranes were 238.6 L/m^2 h and 222.41 L/m^2 h for MMM_1 and MMM_2 which are 9.3-fold and 8.7-fold, respectively, higher than that of the neat PS membrane (M_0). Meanwhile, the rejection of the fouling-inducing model (BSA) has declined from 96.61% in the case of M_0 to 41.9% and 47.6% for MMM_1 and MMM_2, respectively, indicating minimized propensity of BSA adsorption on the membrane surface and consequently reduced fouling. These parameters are in accordance with the results of fouling indices (flux recovery ratio (FRR), total (F_t), reversible (F_r), and irreversible (F_{ir}) fouling) of modified membranes. The FRR% has greatly increased for MMMs as compared to M_0. In contrary, all types of fouling have remarkably reduced for MMMs in comparison to M_0. In addition, the ion-exchange capacity (IEC), as investigated for the nitrate anion, of the $PICCSB_1$-incorporated membrane (MMM_1) is ~34% and ~14% higher than that of the native PS membrane (M_0) and $PICCSB_2$-supported membrane (MMM_2), respectively. In essence, PICCSBs act as excellent membrane-upgrading modifiers for denitrification and wastewater treatment applications. The novelty of this study can be highlighted in the following achievements; (ii) fabrication, for the first time, of dual (ammonium/pyridinium) ionic liquid crosslinking agents for chitosan, to give (poly(ionic) cross-linked chitosan Schiff bases (PICCSBs)), (ii) PICCSBs have effectively acted as synergistic hydrophilicity-modulators, antifouling, and pore-forming/stabilizing additives for a PS ultrafiltration membrane and thus increase its pure water throughput.

Funding

This research did not receive any specific grant from funding agencies in the public, commercial, or not-for-profit sectors.

CRediT authorship contribution statement

Reda F. M. Elshaarawy: Conceptualization, Methodology, Software, Data curation, Validation, Visualization, Writing - Original Draft, Writing - Review & Editing.

Reda M. Abd El-Aal; Conceptualization, Supervision, Visualization.

Fatma H.A. Mustafa: Conceptualization, Software, Data curation, Methodology, Writing - Original Draft.

Ahmed E. Borai: Conceptualization, Methodology, Software, Data curation, Validation.

Stephan Schmidt: Supervision, Software, Data curation,

Christoph Janiak: Supervision, Writing - Original Draft, Writing - Review & Editing.

Declaration of competing interest

All authors show no conflict of interest.

Acknowledgment

The authors would like to thank Dr. Janina Dechnik and Dr. Sandra Nießing, Institut für Anorganische Chemie und Strukturchemie, Heinrich-Heine Universität Düsseldorf, 40204 Düsseldorf, Germany, for their generous efforts in supporting this work.

Appendix A. Supplementary data

The experimental methods, spectral data, and other studies associated with this article are available with the article through the journal Web site. Supplementary data to this article can be found online at doi:10.1016/j.ijbiomac.2020.12.186.

References

[1] N.R. Bond, R.M. Burrows, M.J. Kennard, S.E. Bunn, Water scarcity as a driver of multiple stressor effects, in: S. Sabater, A. Elosegi, R. Ludwig (Eds.), Multiple Stressors in River Ecosystems, Elsevier 2019, pp. 111–129.

[2] A. Bhattacharya, A. Bhattacharya, Nitrogen-use efficiency under changing climatic conditions, Changing climAte and Resource Use Efficiency in Plants, Academic Press 2019, pp. 181–240.

[3] M.L. Brusseau, M. Ramirez-Andreotta, I.L. Pepper, J. Maximillian, Environmental impacts on human health and well-being, in: M.L. Brusseau, I.L. Pepper, C.P. Gerba (Eds.), Environmental and Pollution Science, third ed.Academic Press 2019, pp. 477–499.

[4] Urban Urgency, Water Caucus Summary, World Water Council (WWC), Marseille, France, https://www.worldwatercouncil.org/sites/default/files/Thematics/Urban_Urgency/ 2009. (Accessed 14 October 2009).

[5] B.S. Lalia, V. Kochkodan, R. Hashaikeh, N. Hilal, A review on membrane fabrication: structure, properties and performance relationship, Desalination. 326 (2013) 77–95, https://doi.org/10.1016/j.desal.2013.06.016.

[6] W. Kamiński, Z. Modrzejewska, Application of chitosan membranes in separation of heavy metal ions, Sep. Sci. Technol. 32 (1997) 2659–2668, https://doi.org/10.1080/01496399708006962.

[7] K.C. Khulbe, T. Matsuura, Removal of heavy metals and pollutants by membrane adsorption techniques, Appl Water Sci 8 (2018) 19, https://doi.org/10.1007/s13201-018-0661-6.

[8] S. Sapna, R. Sharma, D. Kumar, Chitosan-based membranes for wastewater desalination and heavy metal detoxification, in: S. Thomas, D. Pasquini, S.-Y. Leu, D.A. Gopakumar (Eds.), Nanoscale Materiala in Water Purification, Elsevier 2019, pp. 799–814.

[9] A. Yusuf, A.D. Sodiq, A. Giwa, J. Eke, O. Pikuda, G.D. Luca, J.L.D. Salvo, S. Chakraborty, A review of emerging trends in membrane science and technology for sustainable water treatment, J. Clean. Prod. 266 (2020) 121867, https://doi.org/10.1016/j.jclepro.2020.121867.

[10] E.O. Ezugbe, S. Rathilal, Membrane technologies in wastewater treatment: a review, Membranes. 10 (2020) 89, https://doi.org/10.3390/membranes10050089.

[11] N. Nady, M.C.R. Franssen, H. Zuilhof, M.S.M. Eldin, R. Boom, K. Schroën, Modification methods for poly(arylsulfone) membranes: a mini-review focusing on surface modification, Desalination. 275 (2011) 1–9, https://doi.org/10.1016/j.desal.2011.03.010.

[12] X. Tan, D. Rodrigue, A review on porous polymeric membrane preparation. Part I: production techniques with polysulfone and poly(vinylidene fluoride), Polymers 11 (2019) 1160, https://doi.org/10.3390/polym11071160.

[13] S. Kheirieh, M. Asghari, M. Afsari, Application and modification of polysulfone membranes, Rev. Chem. Eng. 34 (2017) 657–693, https://doi.org/10.1515/revce-2017-0011.
[14] D. Rana, T. Matsuura, Surface modifications for antifouling membranes, Chem. Rev. 110 (2010) 2448–2471, https://doi.org/10.1021/cr800208y.
[15] Y.G. Dave, A.V.R. Reddy, Preparation, characterization, acid stability and organic fouling of poly(acrylonitrile-co-methacrylic acid) ultrafiltration membranes, Desalination. 282 (2011) 9–18, https://doi.org/10.1016/j.desal.2011.08.055.
[16] J.R. Werber, C.O. Osuji, M. Elimelech, Materials for next-generation desalination and water purification membranes, Nat. Rev. Mater. 1 (2016) 16018, https://doi.org/10.1038/natrevmats.2016.18.
[17] M.S. Diallo, Water treatment by dendrimer-enhanced filtration: principles and applications, in: A. Street, R. Sustich, J. Duncan, N. Savage (Eds.), Nanotechnology Applications for Clean Water, second ed.William Andrew Publishing 2014, pp. 227–239.
[18] A.J. Sanjari, M. Asghari, A review on chitosan utilization in membrane synthesis, ChemBioEng Rev. 3 (2016) 134–158, https://doi.org/10.1002/cben.201500020.
[19] U. Fathanah, I. Machdar, M. Riza, N. Arahman, M.R. Lubis, M. Yusuf, J. Rekayasa, K. dan Lingkungan, The Improvement of hydrophilic property of polyethersulfone membrane with chitosan as additive, J. Chem. Eng. Environ. 15 (2020) 53–61, https://doi.org/10.23955/rkl.v15i1.15916.
[20] F. Ahmadi, Z. Oveisi, S.M. Samani, Z. Amoozgar, Chitosan based hydrogels: characteristics and pharmaceutical applications, Res. Pharm. Sci. 10 (2015) 1–16.
[21] E.I. Rabea, M.E.-T. Badawy, C.V. Stevens, G. Smagghe, W. Steurbaut, Chitosan as antimicrobial agent: applications and mode of action, Biomacromol. 4 (2003) 1457–1465, https://doi.org/10.1021/bm034130m.
[22] C. Liu, R. Bai, L. Nan, Sodium Tripolyphosphate (TPP) crosslinked chitosan membranes and application in humic acid removal, AIChE Annual Meeting, Conference Proceedings 2004, pp. 7147–7160.
[23] Y. Song, Q. Hu, T. Li, Y. Sun, X. Chen, J. Fan, Fabrication and characterization of phosphorylated chitosan nanofiltration membranes with tunable surface charges and improved selectivities, Chem. Eng. J. 352 (2018) 163–172, https://doi.org/10.1016/j.cej.2018.07.010.
[24] J. Ostrowska-Czubenko, M. Gierszewska, M. Pieróg, pH-responsive hydrogel membranes based on modified chitosan: water transport and kinetics of swelling, J. Polym. Res. 22 (2015) 153, https://doi.org/10.1007/s10965-015-0786-3.
[25] R. Antony, T. Arun, S. Theodore, D. Manickam, A review on applications of chitosan-based Schiff bases, Int. J. Biol. Macromol. 129 (2019) 615–633, https://doi.org/10.1016/j.ijbiomac.2019.02.047.
[26] R.F.M. Elshaarawy, F.H.A. Mustafa, A. Herbst, A.E.M. Farag, C. Janiak, Surface functionalization of chitosan isolated from shrimp shells, using salicylaldehyde ionic liquids in exploration for novel economic and ecofriendly antibiofoulants, RSC Adv. 6 (2016) 20901–20915, https://doi.org/10.1039/C5RA27489C.
[27] P.S. Bakshi, D. Selvakumar, K. Kadirvelu, N.S. Kumar, Chitosan as an environment friendly biomaterial – a review on recent modifications and applications, Int. J. Biol. Macromol. 150 (2020) 1072–1083, https://doi.org/10.1016/j.ijbiomac.2019.10.113.
[28] R.F.M. Elshaarawy, H. Abd El-Azim, W.H. Hegazy, F.H.A. Mustafa, T.A. Talkhan, Poly (ammonium/pyridinium)-chitosan Schiff base as a smart biosorbent for scavenging of Cu2+ ions from aqueous effluents, Polym. Test. 83 (2019) 106244, https://doi.org/10.1016/j.polymertesting.2019.106244.
[29] R.F.M. Elshaarawy, A.A. Refaee, E.A. El-Sawi, Pharmacological performance of novel poly-(ionic liquid)-grafted chitosan-N-salicylidene Schiff bases and their complexes, Carbohydr. Polym. 146 (2016) 376–387, https://doi.org/10.1016/j.carbpol.2016.03.017.
[30] R.F.M. Elshaarawy, F.H.A. Mustafa, L. van Geelen, A.E.A. Abou-Taleb, H.R.Z. Tadros, R. Kalscheuer, C. Janiak, Mining marine shell wastes for polyelectrolyte chitosan antibiofoulants: fabrication of high-performance economic and ecofriendly antibiofouling coatings, Carbohydr. Polym. 172 (2017) 352–364, https://doi.org/10.1016/j.carbpol.2017.05.059.
[31] R.F.M. Elshaarawy, J. Dechnik, H.M.A. Hassan, D. Dietrich, M.A. Betiha, S. Schmidt, C. Janiak, Novel high throughput mixed matrix membranes embracing poly ionic liquid-grafted biopolymer: fabrication, characterization, permeation and antifouling performance, J. Mol. Liq. 266 (2018) 484–494, https://doi.org/10.1016/j.molliq.2018.06.100.
[32] R.F.M. Elshaarawy, L.A. Ismail, M.Y. Alfaifi, M.A. Rizk, E.E. Eltamany, C. Janiak, Inhibitory activity of biofunctionalized silver-capped N-methylated water-soluble chitosan thiomer for microbial and niofilm infections, Int. J. Biol. Macromol. 152 (2020) 709–717, https://doi.org/10.1016/j.ijbiomac.2020.02.284.
[33] R.F.M. Elshaarawy, G.A. Seif, M.E. El-Naggar, T.B. Mostafa, E.A. El-Sawi, *In-situ* and *ex-situ* synthesis of poly-(imidazolium vanillyl)-grafted chitosan/silver nanobiocomposites for safe antibacterial finishing of cotton fabrics, Eur. Polym. J. 116 (2019) 210–221, https://doi.org/10.1016/j.eurpolymj.2019.04.013.
[34] O. Iguerb, C. Poleunis, F. Mazéas, C. Compère, P. Bertrand, Antifouling properties of poly(methyl methacrylate) films grafted with poly(ethylene glycol) monoacrylate immersed in seawater, Langmuir. 24 (2008) 12272–12281, https://doi.org/10.1021/la801814u.
[35] L. Liu, D.Y.W. Di, H. Park, M. Son, H.-G. Hur, H. Choi, Improved antifouling performance of polyethersulfone (PES) membrane via surface modification by CNTs bound polyelectrolyte multilayers, RSC Adv. 5 (2015) 7340–7348, https://doi.org/10.1039/C4RA14113J.
[36] C.N. Costa, V.G. Teixeira, M.C. Delpech, J.V.S. Souza, M.A.S. Costa, Viscometric study of chitosan solutions in acetic acid/sodium acetate and acetic acid/sodium chloride, Carbohydr. Polym. 133 (2015) 245–250, https://doi.org/10.1016/j.carbpol.2015.06.094.
[37] M.Y. Alfaifi, J. Alkabli, R.F.M. Elshaarawy, Suppressing of milk-borne pathogenic using new water-soluble chitosan-azidopropanoic acid conjugate: targeting milk-preservation quality improvement, Int. J. Biol. Macromol. 164 (2020) 1519–1526, https://doi.org/10.1016/j.ijbiomac.2020.07.200.
[38] A.G.B. Pereira, E.C. Muniz, Y.-L. Hsieh, 1H NMR and 1H–13C HSQC surface characterization of chitosan–chitin sheath-core nanowhiskers, Carbohydr. Polym. 123 (2015) 46–52, https://doi.org/10.1016/j.carbpol.2015.01.017.
[39] K. Enomoto, J.A. LaVerne, Reactions of hydrated electrons with pyridinium salts in aqueous solutions, J. Phys. Chem. A 112 (2008) 12430–12436, https://doi.org/10.1021/jp8074332.
[40] X. Duan, C. Wang, T. Wang, X. Xie, X. Zhou, Y. Ye, A polysulfone-based anion exchange membrane for phosphoric acid concentration and purification by electrodialysis, J. Membr. Sci. 552 (2018) 86–94, https://doi.org/10.1016/j.memsci.2018.02.004.
[41] M. Kumar, D. McGlade, M. Ulbricht, J. Lawler, Quaternized polysulfone and graphene oxide nanosheet derived low fouling novel positively charged hybrid ultrafiltration membranes for protein separation, RSC Adv. 5 (2015) 51208–51219, https://doi.org/10.1039/C5RA06893B.
[42] J. Li, Z. Cui, R. Tao, S. Yang, M. Hu, C. Matindi, N.N. Gumbi, X. Ma, Y. Hu, K. Fang, J. Li, Tailoring polyethersulfone/quaternary ammonium polysulfone ultrafiltration membrane with positive charge for dye and salt selective separation, J. Polym. Sci. 58 (2020) 2603–2618, https://doi.org/10.1002/pol.20200028.
[43] M.J. Ariza, J. Benavente, Streaming potential along the surface of polysulfone membranes: a comparative study between two different experimental systems and determination of electrokinetic and adsorption parameters, J. Membr. Sci. 190 (2001) 119–132, https://doi.org/10.1016/S0376-7388(01)00430-6.
[44] J. Liu, J. Cheng, X. Ma, X. Zhou, H. Xiang, Photophysical properties and pH sensing applications of luminescent salicylaldehyde derivatives, Res. Chem. Intermed. 42 (2016) 5027–5048, https://doi.org/10.1007/s11164-015-2343-4.
[45] F. Karas, J. Hnát, M. Paidar, J. Schauer, K. Bouzek, Determination of the ion-exchange capacity of anion-selective membranes, Int. J. Hydrog. Energy 39 (2014) 5054–5062, https://doi.org/10.1016/j.ijhydene.2014.01.074.
[46] M. Baghodrat, F. Mehria, S. Rowshanzamir, Electrochemical performance and enhanced nitrate removal of homogeneous polysulfone-based anion exchange membrane applied in membrane capacitive deionization cell, Desalination. 496 (2020) 114696, https://doi.org/10.1016/j.desal.2020.114696.
[47] Q. Gao, C.-Z. Wang, S. Liu, D. Hanigan, S.-T. Liu, H.-Z. Zhao, Ultrafiltration membrane microreactor (MMR) for simultaneous removal of nitrate and phosphate from water, Chem. Eng. J. 355 (2019) 238–246, https://doi.org/10.1016/j.cej.2018.08.137.
[48] H. Koulivand, A. Shahbazi, V. Vatanpour, M. Rahmandoust, Development of carbon dot-modified polyethersulfone membranes for enhancement of nanofiltration, permeation and antifouling performance, Sep. Purif. Technol. 230 (2020) 115895, https://doi.org/10.1016/j.seppur.2019.115895.
[49] A.R. Alawady, A.A. Alshahrani, T.A. Aouak, N.M. Alandisa, Polysulfone membranes with CNTs/chitosan biopolymer nanocomposite as selective layer for remarkable heavy metal ions rejection capacity, Chem. Eng. J. 388 (2020) 124267, https://doi.org/10.1016/j.cej.2020.124267.
[50] R. Kumar, A.M. Isloor, A.F. Ismail, Preparation and evaluation of heavy metal rejection properties of polysulfone/chitosan, polysulfone/N-succinyl chitosan and polysulfone/N-propylphosphonyl chitosan blend ultrafiltration membranes, Desalination. 350 (2014) 102–108, https://doi.org/10.1016/j.desal.2014.07.010.
[51] M. Kumar, D. McGlade, M. Ulbricht, J. Lawler, Quaternized polysulfone and graphene oxide nanosheet derived low fouling novel positively charged hybrid ultrafiltration membranes for protein separation, RSC Adv. 5 (2015) 51208–51219, https://doi.org/10.1039/C5RA06893B.